Korean J. Chem. Eng., 40(5), 1045-1054 (2023)
DOI: 10.1007/s11814-022-1315-9

pISSN: 0256-1115
eISSN: 1975-7220

Onset and growth of gravitational instability in an isolated porous medium: Linear and nonlinear analyses

Min Chan Kim†

Department of Chemical Engineering, Jeju National University, Jeju 63243, Korea
(*Received 20 August 2022 • Accepted 10 October 2022*)

Abstract−Linear and nonlinear analyses were conducted to study the onset and growth of gravitational instability in an isolated porous medium. By considering the dissolution capacity of the isolated system, base concentration profiles were obtained analytically. Based on this base concentration field, linear stability equations were derived under the linear stability theory. The present stability analysis predicts that an isolated system is more stable than the conventional open system. In addition, the dissolution capacity of the isolated system suppresses the onset of instability. Unlike the previous study, the minimum Darcy-Rayleigh number to induce gravitational instability exists and it is a strong function of the dissolution capacity. However, the critical conditions for the high Darcy-Rayleigh number system are insensitive to the dissolution capacity. Based on the results of the linear analysis and the analytically obtained base concentration profile, fully nonlinear numerical simulations were also conducted for the case of $Ra=10^3$. The vertical development of the instability motion and the dissolution flux are significantly suppressed in the high dissolution capacity systems.

Keywords: Gravitational Instability, Isolated System, Dissolution Capacity, Linear Stability Analysis, Numerical Simulation

INTRODUCTION

Carbon dioxide sequestration in deep geological formations has been considered as one of the most promising long-term CO_2 storage strategies [1]. In this CO_2 geological sequestration process, supercritical CO_2 forms an immiscible CO_2-rich gas phase that is lighter than the aqueous brine. This gaseous CO_2 accumulates at the top of the storage formation and gradually dissolves into subsurface brine saturated in the porous formations. Unlike other atmospheric gases, the dissolved CO_2 increases the density of the brine, makes the fluid system gravitationally unstable, and leads to the convective overturn. This convective overturn enhances the CO_2 dissolution process, hence contributes to the long-term storage of CO_2. Thus, many researchers have revisited the stability analysis in the horizontal porous layer, which has been known as the Horton-Rogers-Lapwood (HRL) problem [2,3].

However, there is a critical difference between the classical HRL problem and the CO_2 geological sequestration problem, i.e., the range of the Darcy-Rayleigh number. It is well-known that in the North Sea reservoir, the Darcy-Rayleigh number is very large, $10^3 \le Ra \le 2.5\times10^4$ [4]. To treat this very large Darcy-Rayleigh number case, by extending Caltagirone's [5] analysis for a thermal system, Ennis-King et al. [6] applied conventional linear stability analysis and energy method to the CO_2 geological sequestration problem. Riaz et al. [7] conducted a linear stability analysis in a self-similar coordinate and insisted that the quasi-steady state approximation (QSSA) in the self-similar boundary-layer coordinate gave a reasonable stability condition for a deep-pool system. Selim and Rees [8] and Kim and Choi [9] also examined the stability using the linear theory in the self-similar boundary-layer coordinate. Recently, Emami-Meybodi [10] analyzed the effects of a capillary transition zone and hydrodynamic dispersion on the onset of gravitational instability in the self-similar domain.

Besides the above theoretical work, a number of direct numerical simulations have been conducted for which instability is triggered by spatial white noise [7], a predetermined spatial shape disturbance [11-13] in the initial concentration profile, through spatial white noise in the porosity and permeability [14,15], or by a numerical round-off error without initial perturbation [16]. Pau et al. [15] also showed that the numerical error can induce the onset of convective motion without the physical fluctuation of porosity and permeability. Daniel et al. [17] showed that the initiation time and the amplitude of initial disturbance play important roles in the onset and the growth of instability motion. In addition, Kim [18] suggested that the initiation time and the amplitude of initial disturbance are closely related quantities.

The above analyses focused on the constant pressure system, where the temporal variation of the gaseous CO_2 pressure of the system can be compensated by the lateral inflow of brine, which will increase the interface of the CO_2-brine. The interface movement effect in the constant pressure system was already considered by Myint and Firoozabadi [19], and Kim [20]. However, as discussed by Akhbari and Hesse [21] and Wen et al. [22], some geological CO_2 sequestration sites are isolated from the ambient hydrogeological system and therefore, are commonly underpressured. This means that natural processes reduce the pressure buildup over time and increase storage security. So, we can model this case as a constant volume system, where the temporal variation of the gaseous CO_2 pressure cannot be avoidable. Wen et al. [22] identified the constant pressure and the constant volume systems as the open and the closed

†To whom correspondence should be addressed.
E-mail: mckim@cheju.ac.kr

systems, respectively. in the present study, to explain the difference between the open and the closed systems, the onset and the growth of gravitational instability in a porous medium is analyzed theoretically and numerically. Linear stability equations are re-derived in a similar domain and solved under the quasi-steady state approximation (QSSA). Based on the linear stability analysis, nonlinear direct numerical simulation is conducted for the intermediate Darcy-Rayleigh number case. Therefore, the present study proposes a new framework to connect the onset of instability in an early time diffusion dominant regime and the nonlinear growth of instability motion in the flux-growth and plume-merging regime.

SYSTEM AND GOVERNING EQUATIONS

The system considered here is a porous medium saturated with gas overlaying Newtonian liquid whose initial concentration of solute (gas component) is C_i. For time t≥0, the horizontal layer of liquid depth, d, experiences absorption through the upper free boundary of interfacial area, A, and fixed volume, V, or constant pressure, $P_{b,i}$. As discussed by Wen et al. [22] and Ho and Hadji [23], the fixed volume (isolated) system is quite different from the constant pressure (open) one. It is natural to assume that there is no mass transfer through upper and lower fixed boundaries. A schematic diagram of the basic system of mass diffusion is shown in Fig. 1. For a high ΔC, buoyancy-driven convection will set in before the concentration field reaches its steady state value. Here ΔC ($=C_{s,i}-C_i$) is the concentration difference with $C_{s,i}=HP_{b,i}$, where H is the quasi-Henry's constant and $P_{b,i}$ is the initial pressure of absorbing gas in the gas phase. For an isotropic and homogeneous porous medium, the governing equations of flow and concentration fields are expressed by employing Darcy's law and the Boussinesq approximation as

$$\nabla\cdot\mathbf{U}=0, \tag{1}$$

$$\frac{\mu}{K}\mathbf{U}=-\nabla P+\mathbf{k}\beta g(C-C_i), \tag{2}$$

$$\varepsilon\frac{\partial C}{\partial t}+\mathbf{U}\cdot\nabla C=\varepsilon\mathcal{D}\nabla^2 C, \tag{3}$$

where **U** is the Darcy velocity, K is the permeability, m is the viscosity, β is the densification coefficient, C is the solute concentration, C_i is the initial solute concentration, g is the gravitational acceleration, ε is the porosity, and $\mathcal{D}$ is the diffusion coefficient. The unit vector in the direction of the gravitational acceleration is **k**. For a conventional open system, it is assumed that the pressure of absorbing gas in the gas phase is constant: $P_b(t)=P_{b,i}$. However, for the present isolated system, by considering the reduction of the moles of gas due to the absorption into the liquid phase, Plevan and Quinn [24] derived the following auxiliary condition:

$$\frac{V}{RT}\frac{dP_b}{dt}=A\left(\varepsilon D\frac{\partial C}{\partial Z}\bigg|_{Z=I}\right) \text{ with } P_b|_{t=0}=P_{b,i}. \tag{4}$$

Recently, Kim et al. [25] and Wen et al. [22] used the above condition in their stability analyses. So, the important parameter to describe the present isolated system is the Darcy-Rayleigh number Ra, and the dissolution capacity Π defined by

$$Ra=\frac{g\beta K\Delta C d}{\varepsilon D\nu} \text{ and } \Pi=\frac{AHRTd}{V},$$

where ν is the kinematic viscosity, A is the interfacial area and R is the gas constant. It should be kept in mind that the dissolution capacity is the new dimensionless parameter to govern both the diffusive and the convective mass transport in the isolated system. Because for the specific gas-liquid pair at the given temperature, the quasi-Henry's H is the thermodynamic constant which cannot be controlled, the limiting case of H=0 is not considered here. By considering the mass balance across the interface, Rongy et al. [26] formulated a general approach for the case of constant volume. Later, by neglecting the effect of the evaporation of liquid, Myint and Firoozabadi [19] suggested the following interface condition:

$$-\frac{dZ_I}{dt}=\frac{\mathcal{D}}{1-C_s(t)}\frac{\partial C}{dZ} \text{ at } Z=-Z_I(t). \tag{5}$$

Like Rees et al's [7] and Slim et al's [27] work, using the scale of time $\varepsilon^2\mathcal{D}\nu^2/(Kg\beta\Delta C)^2$, length $\varepsilon\mathcal{D}\nu/(g\beta\Delta CK)$, velocity $Kg\beta\Delta C/\nu$, and concentration ΔC, the above equations are non-dimensionalized as

$$\nabla\cdot\mathbf{u}=0, \tag{6}$$

$$\mathbf{u}=-\nabla p+\mathbf{k}c, \tag{7}$$

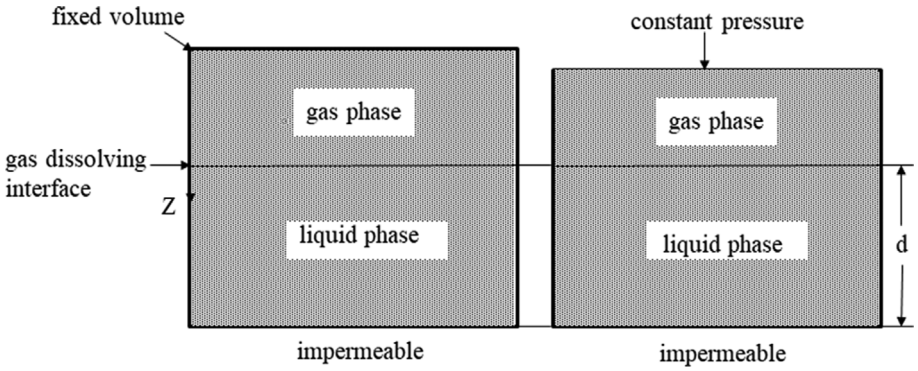

Fig. 1. Schematic diagram of the systems considered here. Gas pressure in the left hand side fixed volume (closed) system is the function of time, whereas the right hand side constant pressure (open) system, as CO_2 dissolves in the brine, the new brine will be filled into the reservoir. Due to this process, the CO_2-brine interface will rise and keep the gas pressure constant.

$$\frac{\partial c}{\partial \tau}+\mathbf{u}\cdot\nabla c=\nabla^2 c, \tag{8}$$

under the following conditions:

$$c=0 \text{ at } \tau=0, \tag{9a}$$

$$\mathbf{k}\cdot\mathbf{u}=0 \text{ and } c=c_s(\tau) \text{ at } z=-z_I(\tau), \tag{9b}$$

$$\mathbf{k}\cdot\mathbf{u}=0 \text{ and } \frac{\partial c}{\partial z}=0 \text{ at } z=Ra. \tag{9c}$$

where Ra has the meaning of the height of the rescaled layer. Slim et al. [27] called the present scale as the advection-diffusion scales, which are appropriate for the case where the instability is localized near the gas-liquid interface. In addition, the following auxiliary condition is needed to describe the temporal evolution of c_s and the interface position z_I:

$$\frac{dc_s}{d\tau}=h\frac{\partial c}{\partial z}\bigg|_{z=-\eta} \text{ with } c_s|_{\tau=0}=1, \tag{10}$$

$$-\frac{dz_I}{d\tau}=\frac{C_s}{1-C_s}\frac{\partial c}{\partial z} \text{ at } z=-z_I(\tau). \tag{11}$$

where $h=\Pi Ra^{-1}$. For the limitng case of $h\to 0$, i.e., $V\to\infty$, the above condition (10) degenerates into

$$c_s=1 \text{ at } z=0. \tag{12}$$

For the system whose boundary concentration is changed abruptly, the stability problem to find the onset condition becomes transient and non-linear. The objective of the present study is to find the critical time t_c to mark the onset of buoyancy-driven instability. Then, the basic diffusion state is represented in dimensionless form by

$$\frac{\partial c_0}{\partial \tau}=\frac{\partial^2 c_0}{\partial z^2}, \tag{13}$$

with the following the initial condition and boundary ones:

$$c_0=0 \text{ at } \tau=0, \tag{14a}$$

$$\frac{dc_0}{d\tau}=h\frac{\partial c_0}{\partial z} \text{ and } c_0|_{\tau=0}=1 \text{ at } z=-z_I, \tag{14b}$$

$$\frac{\partial c_0}{\partial z}=0 \text{ at } z=Ra. \tag{14c}$$

For the limitng case of $h\to 0$, the conditions (14b) are reduced as

$$c_0=1 \text{ at } z=-z_I. \tag{15}$$

For this limting cases of $h\to 0$ and $z_I\to 0$, the above equations can be solved by using the Laplace transform as follows [8]:

$$c_0(\tau,\zeta)=\sum_{n=0}^{\infty}(-1)^n\left\{\operatorname{erfc}\left(\frac{\zeta}{2}+\frac{n}{\sqrt{\tau}}Ra\right)+\operatorname{erfc}\left(\frac{n+1}{\sqrt{\tau}}Ra-\frac{\zeta}{2}\right)\right\}, \tag{16}$$

where $\zeta=z/\sqrt{\tau}$. In addition, for the deep-pool system where δ_C ($\propto\sqrt{\tau}$)<<Ra, the domain can be considered semi-infinite in the positive z-direction, and the base concentration profile is reduced to

$$c_0(\zeta)=\operatorname{erfc}\left(\frac{\zeta}{2}\right), \tag{17}$$

which is known as the early time Lévêque type solution for the open system. Here, the length $\delta_C(\tau)$, within which c_0 is appreciably non-zero, is the so-called solutal penetration depth of the diffusive boundary layer. For the case of $P_b(t)=P_{b,i}$, i.e., $h\to 0$, by considering the effect of the movement of the interface, Myint and Firoozabadi [19] and Kim [20] conducted systematic stability analyses.

For the non-zero h case, following Wen et al's [22] approach, we can obtain the Laplace transform of the base concentration as

$$\mathcal{L}\{c_0(\tau,z)\}=\bar{c}_0(s,z)=\frac{\cosh(\sqrt{s}(Ra-z))}{s\cosh\{\sqrt{s}(Ra+z_I)\}+h\sqrt{s}\sinh\{\sqrt{s}(Ra+z_I)\}}. \tag{18}$$

Because we cannot find the inverse transform of the above variable as a simple analytic function, by using the residue theorem we can get the base concentration as

$$c_0(\tau,z)=\mathcal{L}^{-1}\{\bar{c}_0(s,z)\}=\sum_{n=0}^{\infty}a_n(z)\exp(s_n\tau), \tag{19}$$

where the simple poles, s_k, of the Eq. (18) are given as the roots of

$$\tan\left\{p_n\left(1+\frac{z_I}{Ra}\right)\right\}=\frac{p_n}{\Pi}, \tag{20}$$

where $p_n=iRa\sqrt{s_n}$. Here, $\mathcal{L}$ and $\mathcal{L}^{-1}$ represent the Laplace transform and the inverse Laplace transform, respectively. In addition, the coefficients of the residues for the simple poles are

$$a_n=\lim_{s\to s_n}(s-s_n)\bar{c}_0(z,s)=\lim_{s\to s_n}\frac{(s-s_n)\cosh(\sqrt{s}(Ra-z))}{s\cosh\{\sqrt{s}(Ra+z_I)\}+h\sqrt{s}\sinh\{\sqrt{s}(Ra+z_I)\}}. \tag{21}$$

The above limits yield the following:

$$a_0=\frac{1}{\Pi+1} \text{ and } a_n(z)=\frac{2h\cos\left(p_n\frac{z+z_I}{Ra}\right)-2p_n\sin\left(p_n\frac{z+z_I}{Ra}\right)}{h^2+h+p_n^2} \text{ for } n\geq 1. \tag{22a\&b}$$

From Eqs. (11) and (19), the interface position z_I can be given

$$\frac{dz_I}{d\tau}=\frac{C_{sat}}{1-C_{sat}}\sum_{n=1}^{\infty}\frac{2p_n^2}{Ra(h^2+h+p_n^2)}\exp\left(\frac{p_n^2}{Ra}\tau\right). \tag{23}$$

It is not easy to solve Eqs. (18)-(23) analytically or numerically because the eigenvalue problem, Eq. (20), and the initial value ordinary differential equation for the interface position, Eq. (23), are cross-linked. However, from Eq. (20), we can assume that the effect of the interface movement is not critical for the case of $z_I/Ra<<1$. Furthermore, as discussed by Myint and Firoozabadi [19], for the case of a CO_2-water mixture $C_s=0.043$ at the interface condition of temperature of 30 °C, and the pressure of 50 bars, and C_s may be as large as 0.08. Using the above interface condition, Myint and Firoozabadi [19] and Kim [20] conducted systematic stability analyses for the case of $P_b(t)=P_{b,i}$ and concluded that the interface movement plays little role in the onset of gravitational instability which is significant for the CO_2-water system, where $C_s\leq 0.08$; however, its effects cannot be negligible for CO_2-hydrocarbones mixtures. Because our primary concern is the effect of the reduction the pressure

buildup of the CO_2-brine system on the onset and the growth of the gravitational instability, we are not going to consider the effect of interface movement by fixing the interface position at z_f=0. This simplification makes the system mathematically tractable without distorting physical reality.

For the fixed interface case, Wen et al. [22] suggested that ten modes (0≤n≤9) are quite enough to express the base concentration field for τ>0.03Ra. Using the above relation, during the diffusion period, the gas phase pressure can be given analytically as

$$P_b(\tau)=P_{b,i}\sum_{n=0}^{\infty}\frac{2h}{h^2+h+p_n^2}\exp(-p_n^2\tau/Ra). \tag{24}$$

In previous studies to determine the diffusivity of various gases in liquids, many researchers [22,23] obtained the inverse Laplace transform of $\bar{c}_0(s, 0)$ numerically to obtain the relation of $P_b(\tau)/P_{b,i}$.

For the limiting case of Ra→∞ and/or τ<<Ra^2, Eq. (18) can be reduced as

$$\mathcal{L}\{c_0(\tau, z)\}=\bar{c}_0(s, z)=\frac{\exp(\sqrt{s}z)}{s+h\sqrt{s}}, \tag{25}$$

and its inverse transform is [25]

$$c_0=\exp(h^{*2}+h^*\zeta)\operatorname{erfc}\left(\frac{\zeta}{2}+h^*\right), \tag{26}$$

where $h^*=h\sqrt{\tau}$. Unlike the open system, we cannot obtain the closed form solution late time solution for the present isolated system. Recently, Wen et al. [22] showed that the present Lévêque and Graetz solutions support each other for π/Ra^2<0.03. In the present study, we used the Graetz solution and the Lévêque solution for the early time and late time regime, respectively.

LINEAR STABILITY ANALYSIS

1. Stability Equations

Under linear stability theory, disturbances are formulated in terms of the concentration disturbance c_1 and the vertical velocity disturbance w_1 by perturbing Eqs. (5)-(7):

$$\bar{\nabla}^2 w_1=\bar{\nabla}_1^2 c_1, \tag{27}$$

$$\frac{\partial c_1}{\partial \tau}+w_1\frac{\partial c_0}{\partial z}=\bar{\nabla}^2 c_1, \tag{28}$$

with the boundary conditions,

$$w_1=c_1=0 \text{ at } z=0, \tag{29a}$$

$$w_1=\frac{\partial c_1}{\partial z}=0 \text{ at } z=Ra_D, \tag{29b}$$

where $\bar{\nabla}^2=\partial^2/\partial z^2+\bar{\nabla}_1^2$ and $\bar{\nabla}_1^2=(\partial^2/\partial x^2+\partial^2/\partial y^2)$. The boundary conditions (29b) correspond to the impermeable condition. Under the Fourier mode analysis, the disturbance quantities are expressed as

$$[w_1, c_1]=[w_1(\tau, z), c_1(\tau, z)]\exp\{i(a_x x+a_y y)\}, \tag{30}$$

where a_x and z_y are with the horizontal wavenumbers in the (x, y)-plane, and $\nabla_1^2=-a^2=-(a_x^2+a_y^2)$.

One of the hardest obstacles of the present problem is that the dominant operator of the conventional (τ, z)-domain, $\partial^2/\partial z^2$ does not have eigenfunctions that are localized around the base-concentration front [7-9]. To resolve this, we transformed the disturbance equations such that the eigenfunctions associated with the streamwise diffusion operator are localized around the base-concentration front. Following a coordinate transformation to the similarity variable of the base state $\zeta=z/\sqrt{\tau}$, in the (τ, ζ)-domain, the disturbance equations are expressed as [7-9],

$$\left(\frac{\partial^2}{\partial\zeta^2}-a^{*2}\right)w_1^*=-a^{*2}c_1^*, \tag{31}$$

$$\tau\frac{\partial c_1^*}{\partial\tau}=\left(\frac{\partial^2}{\partial\zeta^2}+\frac{\zeta}{2}\frac{\partial}{\partial\zeta}-a^{*2}\right)c_1^*-\sqrt{\tau}\frac{\partial c_0}{\partial\zeta}w_1^*, \tag{32}$$

with the boundary conditions,

$$w_1^*=c_1^*=0 \text{ at } \zeta=0, \tag{33a}$$

$$w_1^*=\frac{\partial c_1^*}{\partial\zeta}=0 \text{ at } \zeta=Ra/\sqrt{\tau}, \tag{33b}$$

where $a^*(=a\sqrt{\tau})$ is the wavenumber rescaled with $\delta_C(\sim\sqrt{\tau})$. The disturbance quantities are transformed as $w_1^*(\tau, \zeta)=w_1(\tau, z)$ and $c_1^*(\tau, \zeta)=c_1(\tau, z)$ in the (τ, ζ)-domain. Note that for the extreme case of Π=0 and $\sqrt{\tau}$<<Ra, where $\partial c_0/\partial\zeta=-1\sqrt{\pi}\exp(-\zeta^2/4)$, the present system of stability Eqs. (31)-(33) becomes parameter-less, and therefore the solution is universal before the fingertips reach the bottom boundary. For this limiting case of Π=0 and $\sqrt{\tau}$<<Ra, Kim and Choi [28] solved this limiting case analytically.

2. Quasi-steady State Approximation

Except for the limiting case of Π=0 and $\sqrt{\tau}$<<Ra, i.e., the parameter-less case, a fully analytic approach is not possible. So, we have to depend on the quasi-steady state approximation (QSSA), where the base concentration profile is frozen at a certain τ, and the disturbance quantities c_1^* and w_1^* are assumed to have the following forms:

$$[c_1^*(\tau, \zeta), w_1^*(\tau, \zeta)]=[c^*(\zeta), w(\zeta)]\exp(\sigma^*\tau). \tag{34}$$

Under this assumption, Eqs. (31)-(33) become

$$\left(\frac{d^2}{d\zeta^2}-a^{*2}\right)w^*=-a^{*2}c^*, \tag{35}$$

$$\sigma^*\tau c^*=\left(\frac{d^2}{d\zeta^2}+\frac{\zeta}{2}\frac{d}{d\zeta}-a^{*2}\right)c^*+\sqrt{\tau}\frac{dc_0}{d\zeta}w^*, \tag{36}$$

under the following boundary conditions:

$$w^*=c^*=0 \text{ at } \zeta=0, \tag{37a}$$

$$w^*=\frac{dc^*}{d\zeta}=0 \text{ at } \zeta=Ra/\sqrt{\tau}. \tag{37b}$$

In the present study, by solving the above stability Eq. (33)-(37), the critical time, τ_c, to induce instability motions is found for a given Ra and Π. To solve the above stability equation, we employed the outward shooting scheme [29]. For the limiting case of Π=0 and $\sqrt{\tau}$<<Ra, the neutral stability curve corresponding σ^*=0 obtained from the present numerical shooting method is compared with Kim and Choi's [28] analytic solution in Fig. 2. This figure shows that the present solution method follows the analytic solution quite well.

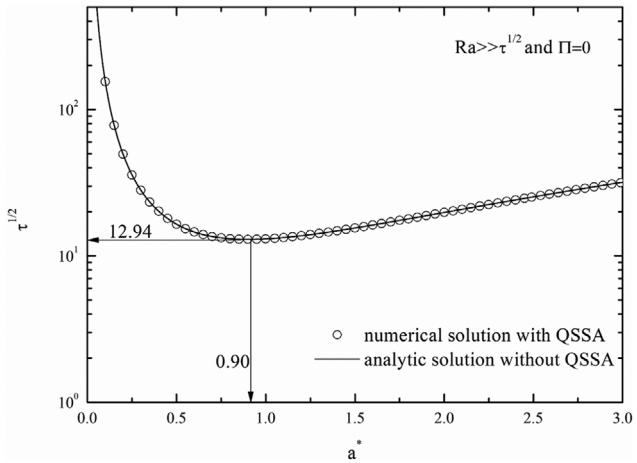

Fig. 2. Comparison of neutral stability curves obtained from the analytic and numerical methods.

NONLINEAR NUMERICAL SIMULATION

1. Formulation and Fourier Spectral Method

In the 2-dimensional (x, z)-domain, so that **u**=(u, w)=($-\partial\psi/\partial z$, $\partial\psi/\partial x$), by taking double curls on Eq. (7) and with the aid of the continuity Eq. (6), the vorticity field can be constructed as

$$\left(\frac{\partial^2}{\partial x^2}+\frac{\partial^2}{\partial z^2}\right)\hat{\psi}=-\frac{\partial \hat{c}_1}{\partial x}, \tag{38}$$

where $\hat{\psi}$ is the stream function. In addition, we expressed the concentration as $c(\tau, x, z)=c_0(\tau, z)+c_1(\tau, x, z)$. Here, $\hat{f}$ represents the odd extension of physical quantity, f, and therefore, we can extend the vertical domain [0, Ra] to [−Ra, Ra]. Through this odd extension, we can use the discrete Fourier transform (DFT) in the present simulation. Then, the convective-diffusion equation can be reduced as

$$\frac{\partial \hat{c}_1}{\partial \tau}=\left(\frac{\partial^2}{\partial x^2}+\frac{\partial^2}{\partial z^2}\right)\hat{c}_1-\hat{j}, \tag{39}$$

where

$$\hat{j}=\frac{\partial \tilde{c}_0}{\partial z}\frac{\partial \hat{\psi}}{\partial x}+\frac{\partial \hat{c}_1}{\partial z}\frac{\partial \hat{\psi}}{\partial x}-\frac{\partial \hat{c}_1}{\partial x}\frac{\partial \hat{\psi}}{\partial z}. \tag{40}$$

Before the fingertips reach the lower boundary, boundary conditions are not important. So, the following Dirichlet boundary conditions are used in the present simulations:

$$\hat{\psi}=\hat{c}_1=0 \text{ at } z=\pm Ra. \tag{41}$$

By applying the discrete Fourier transform into Eqs. (38)-(41), we can obtain the following spectral equations:

$$(k_p^2+k_q^2)\,\Psi_{pq}=ik_qC_{pq}, \tag{42}$$

$$\frac{dC_{pq}}{d\tau}=-(k_p^2+k_q^2)C_{pq}-J_{pq}, \tag{43}$$

where Ψ, C and J are the DFT of $\hat{\psi}$, $\hat{c}$ and $\hat{j}$. The solution of Eq. (43) can be expressed as

$$C_{pq}(\tau+\Delta\tau)=C_{pq}(\tau)$$
$$-\exp\{-(k_p^2+k_q^2)\tau\}\int_{\tau}^{\tau+\Delta\tau}J_{pq}\exp\{(k_p^2+k_q^2)\tau'\}\,d\tau', \tag{44}$$

After the Fourier components Ψ_{pq} and C_{pq} were obtained by solving the above equations, their physical components $\hat{\psi}_{mn}$ and $\hat{c}_{mn}$ were obtained by taking an inverse discrete Fourier transform (IDFT) on their Fourier components. In the present study, we used the Adams-Bashford predictor-corrector method to calculate the integral of Eq. (44). Detailed procedures are well explained by Kim [30,31].

2. Nonlinear Simulations

In the present study, we set the calculation domain as [0, 2Ra]×[−Ra, Ra], and used 2,048×2,048 collocation points. From Kim and Choi's [9] initial growth rate analysis, the following initial conditions are employed:

$$\hat{c}_1(\tau_i, x, z)=\delta_i\frac{1}{\sqrt{2\sqrt{\pi}}}\zeta_i\exp\left(-\frac{\zeta_i^2}{4}\right)\text{rand}(x), \tag{45a}$$

$$\psi(\tau_i, x, z)=0, \tag{45b}$$

where δ_i means the initial disturbance level at the initiation time τ_i, $\zeta_i=z/\sqrt{\tau_i}$, and rand(x) is the pseudo-random number uniformly distributed between −1 and 1. For the region of $\tau\sim0$, the base concentration gradients show non-analytic features and lead to bad convergence properties. For this reason, at all the non-linear numerical simulations, the disturbance given in Eq. (45) is introduced as $\tau_i=0.1$.

Here, we are interested in the enhancement of mixing or mass transfer driven by the instability motion. Let us consider the mass transfer rate. The dimensionless mass fluxes at the front z=0, J, which can be written as the sum of contributions from the base diffusion state, J_0, and the convective motion, J_1:

$$J=J_0+J_1. \tag{46}$$

The diffusional flux can be computed explicitly from the base concentration profile as

$$J_0=-\left.\frac{\partial c_0}{\partial z}\right|_{z=0}. \tag{47}$$

The fluxes from the convective motion are obtained as [32]

$$J_1=\left\langle-\left.\frac{\partial c_1}{\partial z}\right|_{z=0}\right\rangle=[\![w_1c_1]\!], \tag{48}$$

where $\langle X\rangle=\frac{1}{2Ra}\int_0^{2Ra}(X)dx$ and $[\![X]\!]=\frac{1}{2Ra}\frac{1}{Ra}\int_0^{2Ra}\int_0^{Ra}(X)dzdx$.

In the present study, following Slim's [13] suggestion, we classify flow regimes as the diffusive where the diffusive forces suppress the convective one, the linear growth where the convective forces are accumulated enough for the convection to start, and the flux growth where convection motions are now apparent and begin to influence mass flux. However, due to inherent limitations of the present Fourier spectral method, i.e., calculation should be stopped before the fingertips reach the lower boundary, we cannot study thoroughly Slim's [13] merging, constant flux and shutdown regimes. For the open system, the effects of the random sequence on the

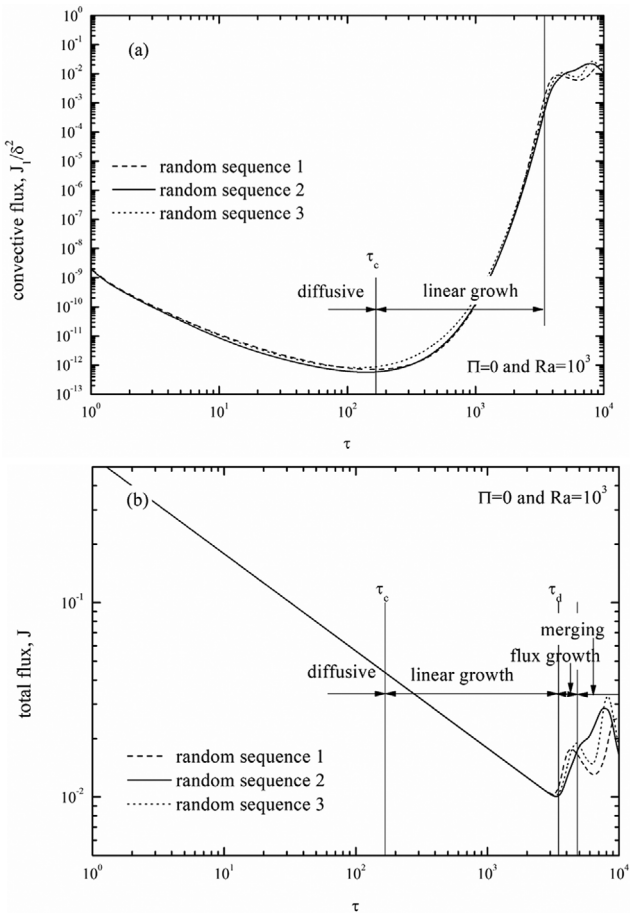

Fig. 3. Effect of a random sequence on (a) the convective flux and (b) the total dissolution flux for the case of Ra=10^3 and Π=0. We employed Eq. (45) with τ_i=0.1 and δ=0.01 as initial conditions.

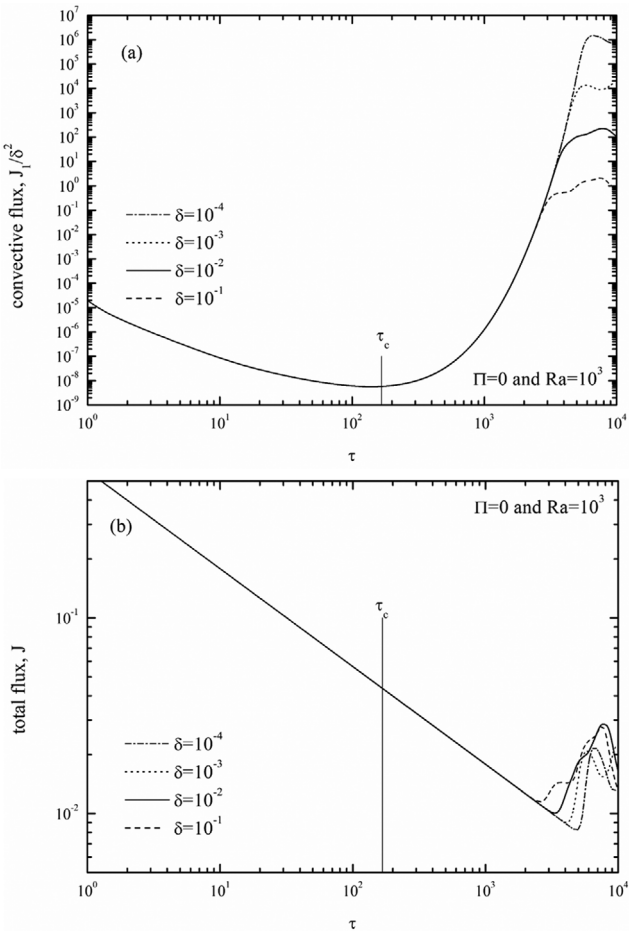

Fig. 4. Effect of the initial amplitude of disturbance on (a) the convective flux and (b) the total dissolution flux for the case of Ra=10^3 and Π=0. We employed Eq. (45) with τ_i=0.1 and various value of δ as initial conditions.

convective flux, J_1, and the total dissolution flux, J, are summarized in Fig. 3. This figure shows that the effect of the shape of the initial condition is not critical except for the flux growth regime. The effect of the initial amplitude of disturbance is given in Fig. 4. As shown in this figure, the growth rate of disturbance is independent of the initial amplitude in the linear growth regime, where the disturbances grow exponentially. However, the deviation time τ_d, from which the growth of disturbance deviates from the exponential growth and the total flux shows its minimum value, is strongly dependent on the initial amplitude. Similar results were also reported by Slim [13]. This initial amplitude dependency means that the temporal evolution of the total flux depends on experimental conditions. The effect of the vertical structure of the initial condition on the temporal evolution of the total flux is summarized in Fig. 5. This figure shows that the vertical structure of the initial condition is not critical if the initial disturbance is an odd function.

Note that in the present non-linear simulation results are somewhat different from those of Selim and Rees's [11]. They introduced the following initial condition rather than present one, Eq. (45):

$$\hat{c}_1(\tau_i, x, z) = \delta_i \eta \exp(-3\eta)\cos kx, \tag{49}$$

where $\eta=\zeta_i/2$. The critical difference between the present and Selim and Rees's [11] simulation is that the lateral periodicity is not fixed in the present study; however, in Selim and Rees's [11] work, the lateral periodicity is fixed by keeping the wavenumber constant. According to Selim and Rees's [11] results, the temporal evolution of the convective and total fluxes is strongly dependent on the wavenumber and is quite different from the present results for a certain wavenumber range. This means that the lateral periodicity plays an important role in the non-linear growth of disturbances.

Because the temporal evolution of the total dissolution flux is quite similar to Shi et al's [33] experimental and numerical work, we used the initial disturbance given in Eq. (45) with τ_i=0.1 and δ=0.01 as initial conditions for the simulations. As shown in Fig. 3(a), τ_c from the linear analysis is comparable with the time from which the norm of c_1 starts to grow. This means that the present linear and nonlinear analyses support each other in the diffusional period. For a certain random sequence, the temporal evolution of the concentration field is given in Fig. 6. As shown in Fig. 6, regularly spaced individual fingers constitute a global velocity field and thus influence one another's motion. After the time of maximum flux, i.e., $\tau \geq 6\times10^3$, fingers begin to interact with neighbors and merge nearby ones. This cell-merging process slightly increases the diffu-

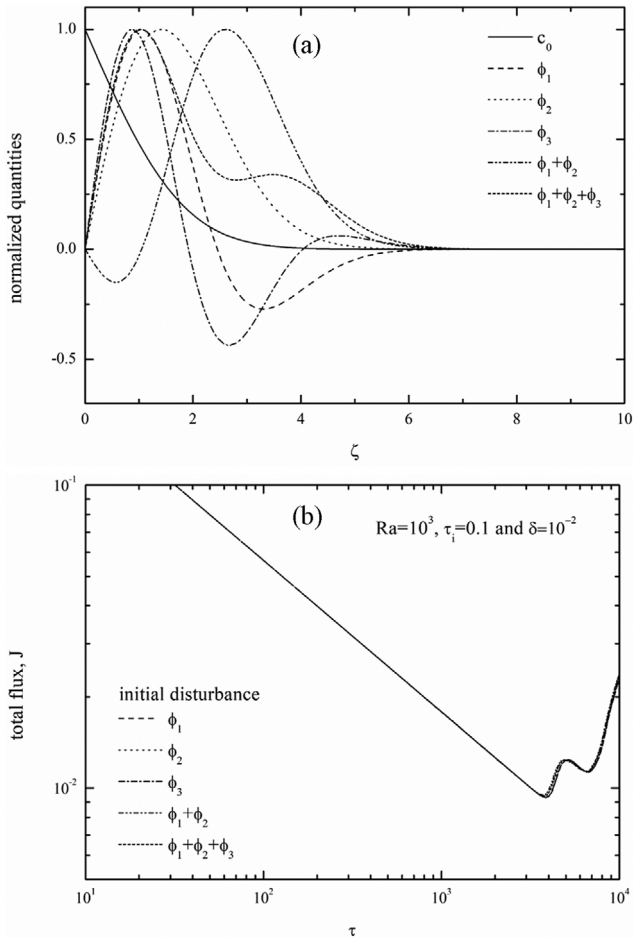

Fig. 5. Effects of the vertical structure of the initial disturbance on the total flux J. (a) vertical structure of equally weighted initial disturbance, (b) temporal evolution of the total flux J for the initial condition given in (a). We employed Eq. (45) with τ_i=0.1 and various value of δ=10^{-2} as initial conditions.

sive layer thickness below the interface (see the concentration field at τ=7×10^3). This results in a decreased concentration gradient in the diffusive layer and thus progressively reduces the dissolution flux. Slim [13] called this regime showing this wavy flux-time relation as the merging regime.

Temporal variations of the total flux summarized in Figs. 3(b) are quite similar to Wen and Hesse's [34] result for Ra=10^3 and the concentration fields featured in Fig. 5 are good agreement with Slim's [13] results for Ra>500. Because we should stop our simulation before the tip of the finger reaches the lower bound of the system, we employed Wen and Hesse's [34] and Slim's [13] results for the quasi-steady state and shutdown regime.

RESULTS AND DISCUSSION

The variation of onset time as a function of Rayleigh number, Ra, and dissolution capacity, Π, is given in Fig. 6. The right-hand side of each curve is the unstable region. As shown in Fig. 7, for the case of $Ra^{-2}\tau_c \le 0.03$, the critical times using the Lévêque type early-time solution represent those using the Graetz type late-time solu-

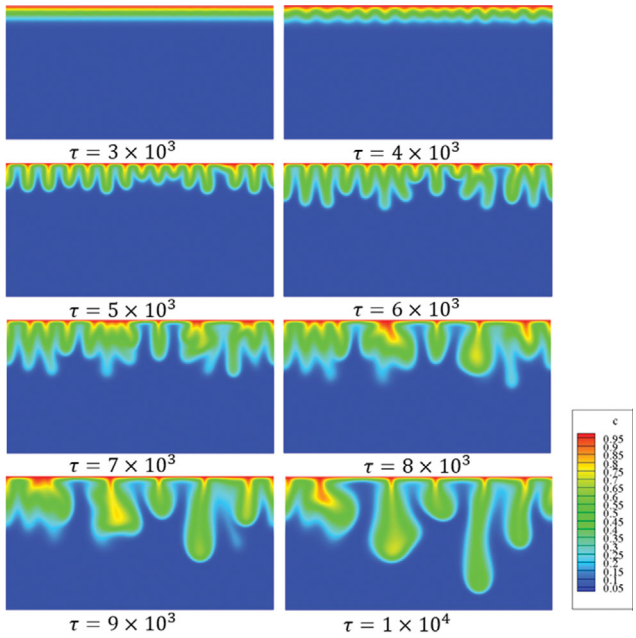

Fig. 6. Snapshots of the concentration field for the case of Ra=10^3 and Π=0.

tion. At a large Ra, the stability of the isolated system is not affected by Π. However, at a small Ra, Π makes the system stable and, therefore, delays the onset of convection due to the reduction of a dissolution flux. Unlike Wen et al.'s [22] stability analysis, the present result shows that the isolated system, $\Pi \neq 0$, is always more stable than the open system, Π=0, regardless of Ra. It is interesting that for the case of Ra≥10^3, the critical time, τ_c, is nearly independent of Π.

The original HRL problem is for the thermal system, where the upper and lower boundaries are kept as isothermal. For this thermal system, the dimensionless temperature is

$$\theta_0 = \sum_{n=0}^{\infty}\left\{\operatorname{erfc}\left(\frac{\zeta}{2}+\frac{n}{\sqrt{\tau}}\mathrm{Ra}\right)-\operatorname{erfc}\left(-\frac{\zeta}{2}+\frac{n+1}{\sqrt{\tau}}\mathrm{Ra}\right)\right\}, \tag{50}$$

and the boundary conditions (37) should be

$$w^* = \theta^* = 0 \text{ at } \zeta = 0, \tag{51a}$$

$$w^* = \theta^* = 0 \text{ at } \zeta = \mathrm{Ra}/\sqrt{\tau}. \tag{51b}$$

Horton and Rogers [2], and Lapwood [3] proved that the critical Darcy-Rayleigh number and corresponding wavenumber are

$$\mathrm{Ra}_c = 4\pi^2 \text{ and } a_c = \pi. \tag{52}$$

As shown in Fig. 7, the present study reproduces the HRL solution quite well, which proves the validity of the present stability analysis.

Recently, Wen et al. [22] introduced a random disturbance within the top diffusion layer at $\tau=\tau_i$, and solved Eqs. (6)-(9) numerically. They employed τ_i=1 for the wide range of Ra. They defined the critical time, τ_c, as the time at which the norm of c_1 starts to grow. Unlike the present study, Wen et al. [22] did not suggest the minimum Darcy-Rayleigh number, below which the convective instability cannot be expected. This minimum Darcy-Rayleigh num-

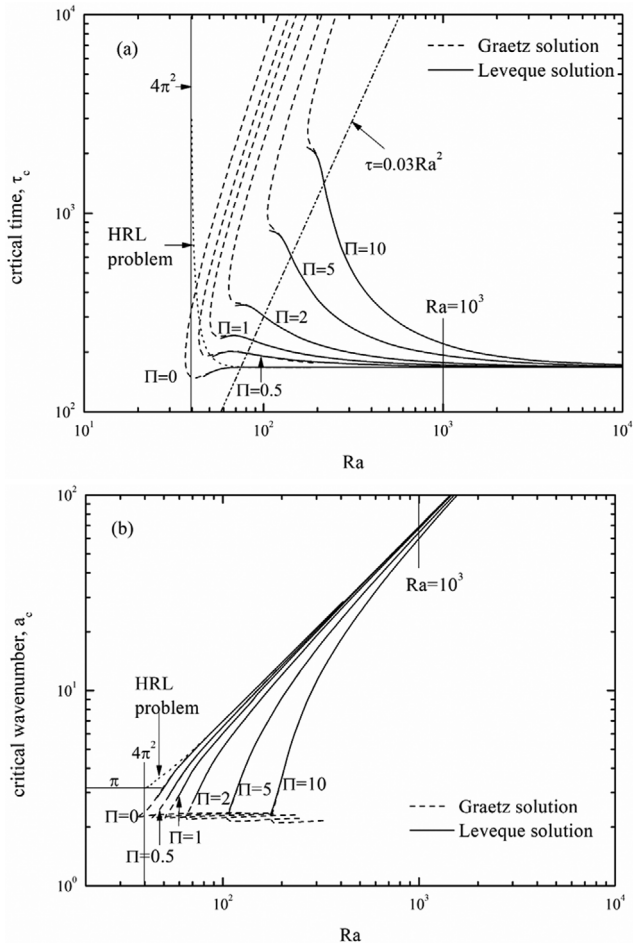

Fig. 7. Critical time (a) and critical wavenumber (b) for the various systems. For the thermal system, we reconstruct the HRL's critical Rayleigh number. For the case of Ra≥10^3, the effect of Π on the critical conditions is less important.

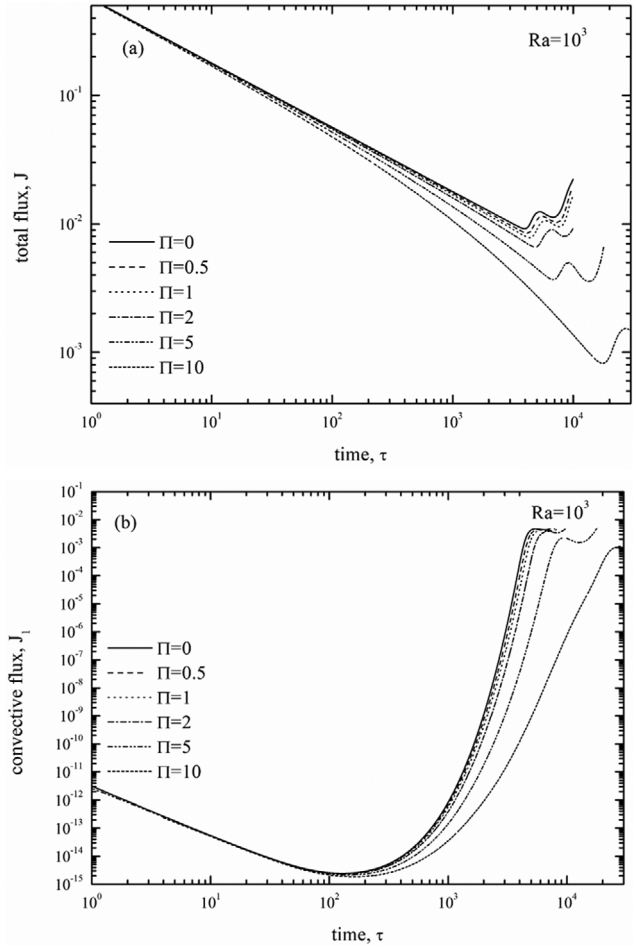

Fig. 8. Effect of the dissolution capacity on the evolution of (a) the total dissolution flux and (b) convective flux for the case of Ra=10^3. We employed Eq. (45) with τ_i=0.1 and δ=0.01 as initial conditions.

ber was also reported by Ennis-King et al. [6]. They explained this Darcy-Rayleigh number by considering the difference between the present system and the thermal system. Due to the reduction of dissolution flux from the negative feedback of the pressure drop in gas, the minimum Darcy-Rayleigh number to induce instability increases as the dissolution capacity increases. However, the effect of the dissolution capacity on the stability characteristics becomes less significant at the high Darcy-Rayleigh number regime.

For the constant pressure system, Slim [13] conducted numerical simulations for 10^2≤Ra≤5×10^4 by introducing the following initial disturbance:

$$c_1(\tau_i, x, z) = \delta_i\sqrt{0.002}z\exp(0.5-0.001z^2)\mathrm{rand}(x), \quad (53)$$

at τ_i=1. According to his simulation results, for the case of Ra≥10^3, there are four Ra-independent regimes: pure diffusion, linear growth, flux growth, and merging, and two Ra-dependent regimes: quasi-steady flux and shut-down. According to Slim's [13] results, transition times between these regimes depend sensitively on the initial disturbance amplitude, δ_i. However, the quasi-steady flux is less so. For the system of Ra=2×10^4, Wen et al. [22] introduced small amplitude random noise at τ_i=25 and traced its impact on the concentration and flow field numerically. They considered the effect of dissolution capacity, Π, on the dissolution flux and concluded that unlike the constant pressure system whose Π=0, there does not exist a quasi-steady flux regime for Π>0. Wen et al. [22] also showed that the diffusion dominant regime, i.e., pure diffusion and linear growth regimes, is not significantly affected by Π, due to the early onset of convection at high Ra.

In the North Sea reservoir, the Darcy-Rayleigh number is 10^3≤Ra≤2.5×10^4. Because Wen et al. [22] focused on the upper limit of the above range, i.e., Ra=2×10^4, we considered the effect of the dissolution capacity, Π, on the convective dissolution for the lower limit of the North Sea reservoir, i.e., Ra=10^3. To compare the open and the isolated systems, the effect of Π on the dissolution flux is summarized in Fig. 8. Unlike Wen et al's [22] work, the dissolution capacity, Π, plays important roles not only in two Ra-dependent regimes but also in the linear growth regime. However, for the case of Ra=10^3, the critical time, τ_c, from which the norm of convective flux starts to grow, is nearly independent of Π, because the variation of gas phase pressure, i.e., the interface concentration, can be negligible for $\tau_i \le \tau \le \tau_c$. As shown in Fig. 7(a), this feature is also expected from the linear stability analysis.

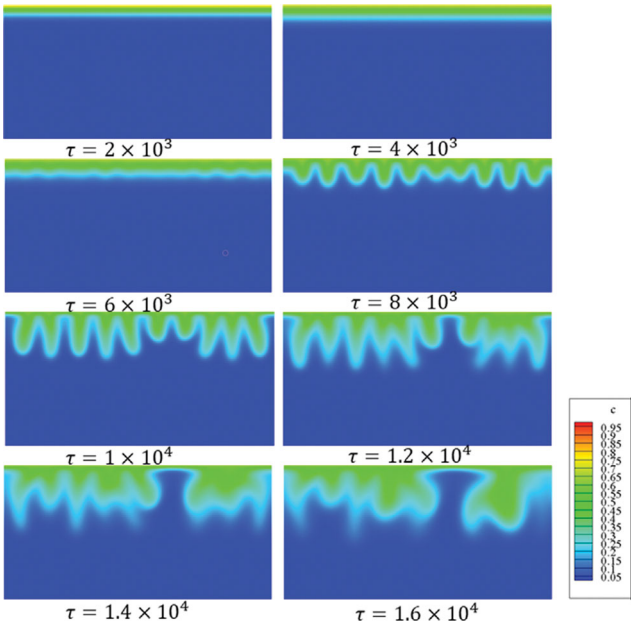

Fig. 9. Snapshots of the concentration field for the case of Ra=10^3 and Π=5.

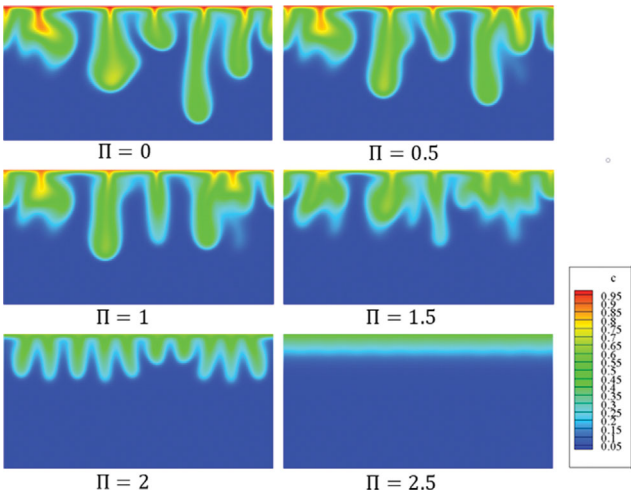

Fig. 10. Effect of the dissolution capacity, Π, on the concentration field for the system of Ra=10^3 at τ=10^4.

The temporal evolution of the concentration field for the case of Π=5 is given in Fig. 9. Unlike the Π=0 system summarized in Fig. 7, where the interface concentration is constant, the significant reduction of the interface concentration and the dissolution flux are clearly observed and, therefore, the growth of disturbance is strongly suppressed. In addition, for the typical North Sea reservoir condition at 90 °C and 300 bar, where Ra≈10^3, the snapshots of concentration fields at τ=10^4 (≈1,290 yrs) are summarized in Fig. 10. For the case of Ra=10^3, Π plays an important role even in the diffusion dominant regime.

CONCLUSIONS

In an isolated porous medium, linear and nonlinear analyses were conducted to study the effect of dissolution capacity, Π, on the onset and growth of gravitational instability. By considering the dissolution capacity of an isolated system, base concentration profiles were obtained analytically by employing the Laplace transform method. Using these base concentration fields, stability equations were derived under linear stability theory, and solved in a similar domain. The present stability analysis predicts that the isolated system is more stable than the conventional open system. In addition, the dissolution capacity of the isolated system suppresses the onset of instability. Based on the results of the linear analysis and the analytically obtained base concentration profile, fully nonlinear numerical simulations were also conducted for the case of Ra=10^3. Unlike the previous study for the very high Darcy-Rayleigh number case, i.e., Ra=2×10^4, Π plays an important role in the diffusion dominant regime and suppresses the vertical development of the instability motion and the dissolution flux for the intermediate Darcy-Rayleigh number case, i.e., Ra=10^3. Due to the inherent limitation of the present Fourier spectral method, we cannot estimate maximum quantity of gas absorbed into liquid phase, which should be estimated by using the previous studies [13,34].

ACKNOWLEDGEMENT

This research was supported by the 2022 scientific promotion program funded by Jeju National University.

REFERENCES

1. B. Metz, O. Davidson, H. C. de Coninck, M. Loos and L. A. Meyer, *IPCC special report on carbon dioxide capture and storage*, Cambridge University Press, Cambridge, U.K. (2005).
2. C. W. Horton and F. T. Rogers, *J. Appl. Phys.*, **16**, 367 (1945)
3. E. R. Lapwood, *Proc. Camb. Phil. Soc.*, **44**, 508 (1948).
4. E. Lindberg and D. Wessel-Berg, *Energy Convers. Manage.*, **38**, S229 (1997).
5. J.-P. Caltagirone, *Quart. J. Mech. Appl. Math.*, **33**, 47 (1980).
6. J. Ennis-King, I. Preston and L. Paterson, *Phys. Fluids*, **17**, 084107 (2005).
7. A. Riaz, M. Hesse, H. A. Tchelepi and F. M. Orr, *J. Fluid Mech.*, **548**, 87 (2006).
8. A. Selim and D. A. S. Rees, *J. Porous Media*, **10**, 1 (2007).
9. M. C. Kim and C. K. Choi, *Phys. Fluids*, **24**, 044102 (2012).
10. H. Emami-Meybodi, *Phys. Fluids*, **29**, 014102 (2017).
11. A. Selim and D. A. S Rees, *J. Porous Media*, **10**, 17 (2007).
12. A. Selim and D. A. S Rees, *J. Porous Media*, **13**, 1039 (2010).
13. A. C. Slim, *J. Fluid Mech.*, **741**, 461 (2014).
14. H. Hassanzadeh M. Pooladi-Darvish and D. W. Keith, *AIChE J.*, **53**, 1121 (2007).
15. G. S. H. Pau, J. B. Bell, K. Pruess, A. S. Almgren, M. J. Lijewski and K. Zhang, *Adv. Water Resour.*, **33**, 443 (2010).
16. Q. Meng and X. Jiang, *Appl. Energy*, **130**, 581 (2014).
17. D. Daniel, N. Tilton and A. Riaz, *J. Fluid Mech.*, **727**, 456 (2013).
18. M. C. Kim, *Chem. Eng. Sci.*, **98**, 255 (2013).
19. P. C. Myint and A. Firoozabadi, *Phys. Fluids*, **25**, 094105 (2013).
20. M. C. Kim, *Int. J. Heat Mass Transfer*, **100**, 779 (2016).

21. D. Akhbari and M. A. Hesse, *Geology*, **45**, 47 (2017).
22. B. Wen, D. Ahkbari, L. Zhang and M. A. Hesse, *J. Fluid Mech.*, **854**, 56 (2018).
23. L. Vo and L. Hadji, *Phys. Fluids*, **29**, 127101 (2017).
24. R. E. Plevan and J. A. Quinn, *AIChE J.*, **12**, 894 (1966).
25. M. C. Kim, D. Y. Yoon and C. K. Choi, *Ind. Eng. Chem. Res.*, **45**, 7321 (2006).
26. L. Rongy, K. G. Haugen and A. Firoozabadi, *AIChE J.*, **58**, 1336 (2012).
27. A. C. Slim, M. M. Bandi, J. C. Miller and L. Mahadevan, *Phys. Fluids*, **25**, 024101 (2013).
28. M. C. Kim and C. K. Choi, *Korean J. Chem. Eng.*, **32**, 2400 (2015).
29. M. C. Kim, *Korean J. Chem. Eng.*, **35**, 364 (2018).
30. M. C. Kim, *Korean Chem. Eng. Res.*, **59**, 138 (2021).
31. M. C. Kim, *Korean J. Chem. Eng.*, **39**, 548 (2022).
32. J. T. H. Andres and S. S. S. Cardoso, *Chaos*, **22**, 037113 (2012).
33. Z. Shi, B. Wen, M. A. Hesse, T. T. Tsotsis abd K. Jessen, *Adv. Water Resour.*, **113**, 100 (2018).
34. B. Wen and M. A. Hesse, Rayleigh fractionation in high-Rayleigh-number solutal convection in porous media, https://arxiv.org/abs/1801.03075.